JACS
JOURNAL OF THE AMERICAN CHEMICAL SOCIETY
Communication
pubs.acs.org/JACS

Synthesis of 4H/fcc-Au@Metal Sulfide Core–Shell Nanoribbons

Zhanxi Fan,[†] Xiao Zhang,[†] Jian Yang,[†] Xue-Jun Wu,[†] Zhengdong Liu,[‡,§] Wei Huang,[‡,§] and Hua Zhang*[,†]

[†]School of Materials Science and Engineering, Nanyang Technological University, 50 Nanyang Avenue, Singapore 639798, Singapore

[‡]Key Laboratory for Organic Electronics and Information Displays & Institute of Advanced Materials (IAM), Jiangsu National Synergetic Innovation Center for Advanced Materials (SICAM), Nanjing University of Posts & Telecommunications (NUPT), 9 Wenyuan Road, Nanjing 210023, China

[§]Key Laboratory of Flexible Electronics (KLOFE) & Institute of Advanced Materials (IAM), Jiangsu National Synergetic Innovation Center for Advanced Materials (SICAM), Nanjing Tech University (NanjingTech), 30 South Puzhu Road, Nanjing 211816, China

Supporting Information

ABSTRACT: Although great advances on the synthesis of Au–semiconductor heteronanostructures have been achieved, the crystal structure of Au components is limited to the common face-centered cubic (fcc) phase. Herein, we report the synthesis of 4H/fcc-Au@Ag_2S core–shell nanoribbon (NRB) heterostructures from the 4H/fcc Au@Ag NRBs via the sulfurization of Ag. Remarkably, the obtained 4H/fcc-Au@Ag_2S NRBs can be further converted to a novel class of 4H/fcc-Au@metal sulfide core–shell NRB heterostructures, referred to as 4H/fcc-Au@MS (M = Cd, Pb or Zn), through the cation exchange. We believe that these novel 4H/fcc-Au@metal sulfide NRB heteronanostructures may show some promising applications in catalysis, surface enhanced Raman scattering, solar cells, photothermal therapy, etc.

Metal–semiconductor heteronanostructures have received great attention because of their unique optical, catalytic and electronic properties, and potential applications in surface enhanced Raman scattering (SERS), photothermal therapy, solar energy conversion and information storage.[1] In particular, Au–semiconductor heteronanostructures have attracted increasing interests as Au nanostructures exhibit excellent chemical stability and strong localized surface plasmon resonance (LSPR), which can significantly enhance the light absorption of semiconductor, and enable the electron transfer from Au to the semiconductor component through the so-called "hot-electron" effect.[2] To date, various Au nanostructures, such as spherical nanoparticles, nanopolyhedra, nanorods, and nanoplates, have been used for the synthesis of Au–semiconductor heteronanostructures.[3] Although great advances have been achieved for the preparation of Au–semiconductor heteronanostructures, the crystal structure of Au components is limited to the common face-centered cubic (fcc) phase. Moreover, the preparation of Au nanoribbon (NRB)–semiconductor heterostructures remains a challenge.

As known, the cation exchange reaction has been demonstrated as a versatility way to modulate the chemical compositions, structures and properties of ionic nanocrystals, especially for the transition metal chalcogenides (TMCs).[4] Due to the relative rigidity of anionic framework of TMC nanocrystals, their sizes and shapes are mostly conserved during the cation exchange.[5] As a result, novel heteronanostructures can be prepared via the cation exchange in TMC nanostructures.[5a,6] Importantly, the cation exchange reaction can also be used for synthesis of Au–semiconductor heteronanostructures through a nonepitaxial growth strategy.[4e] For instance, small fcc-Au@CdS core–shell nanospheres have been prepared from the fcc-Au@Ag_2S nanospheres via the cation exchange of Ag^+ with Cd^{2+} ions.[4e]

Gold nanostructures normally crystallize in the fcc phase. Recently, for the first time, our group reported the synthesis of hexagonal close-packed (hcp, 2H type) Au square sheets,[7] and then the 4H hexagonal Au NRBs.[8] Different from the common fcc phase, which shows a typical stacking sequence of "ABC" along the close-packed direction of $[111]_f$, the 2H and 4H structures of Au demonstrate characteristic stacking sequences of "AB" and "ABCB" along the close-packed directions of $[001]_{2H}$ and $[001]_{4H}$, respectively. Importantly, through the epitaxial growth of noble metals (e.g., Ag, Pd or Pt) on Au square sheets or NRBs, novel Au@noble metal core–shell nanostructures were obtained,[2d,8,9] including the alternating 4H/fcc Au@Ag NRBs.[8] Due to the small lattice mismatch, it is relatively easy to realize the growth of Ag, Pd and Pt on the surface of 4H Au NRBs.[8] However, considering the large lattice mismatch between Au and semiconductors, e.g., Ag_2S, CdS, PbS, and ZnS,[4e] it remains quite difficult to prepare non-fcc Au–semiconductor heteronanostructures via the direct growth of semiconductor nanomaterials on 4H Au NRBs. Note that Au–semiconductor heteronanostructures exhibit superior properties (e.g., photocatalytic activity) in comparison with their individual components, which is derived from the synergistic effects between Au and semiconductor nanostructures.[1b,2a–c] Herein, for the first time, we report the synthesis of 4H/fcc-Au@Ag_2S core–shell NRBs via the sulfurization of 4H/fcc Au@Ag NRBs. Then, a series of 4H/fcc-Au@metal sulfide core–shell NRBs, referred to as 4H/fcc-Au@MS (M = Cd, Pb, or Zn), can be prepared from the obtained 4H/fcc-Au@Ag_2S NRBs through the cation exchange reaction. The detailed structure characterization and analyses prove that the polycrystalline metal sulfide shells are coated on the 4H/fcc Au cores.

Received: June 20, 2015
Published: August 19, 2015

DOI: 10.1021/jacs.5b06405
J. Am. Chem. Soc. 2015, 137, 10910–10913

The alternating 4H/fcc Au@Ag NRBs were prepared based on our previously reported method.[8] Transmission electron microscope (TEM) and scanning TEM-energy dispersive X-ray spectroscopy (STEM-EDS) analyses confirmed the structure of alternating 4H/fcc of Au@Ag NRBs with average Au/Ag atomic ratio of 1.0/1.6 (Figures S1, S2), consistent with our previous report.[8] The obtained 4H/fcc Au@Ag NRBs were then used to synthesize 4H/fcc-Au@metal sulfide core−shell NRBs. The detailed experiments are described in the Supporting Information. Briefly, the sulfurization of Ag in alternating 4H/fcc Au@Ag NRBs was first carried out to synthesize 4H/fcc-Au@Ag_2S NRBs, which were then used to prepare 4H/fcc-Au@MS (M = Cd, Pb, or Zn) NRBs via the cation exchange reaction (Scheme 1).

Scheme 1. Schematic Illustration for Synthesis of 4H/fcc-Au@Metal Sulfide Core−Shell NRB Heterostructures

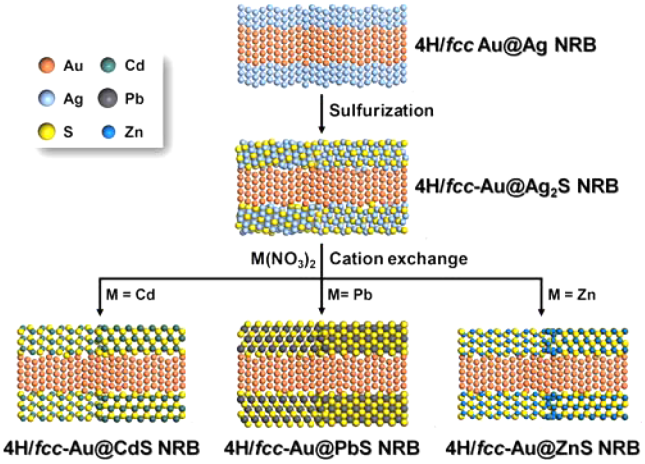

As shown in Scheme 1, 4H/fcc-Au@Ag_2S heteronanostructures were obtained via the sulfurization of 4H/fcc Au@Ag NRBs at 50 °C (see the Experimental Section in Supporting Information for details). The Ag_2S shell with thickness of about 4.5 nm is formed on the Au NRB core (Figure 1a,b). The selected area electron diffraction (SAED) pattern of the obtained Au@Ag_2S NRBs suggests that the Au core and Ag_2S shell are alternating 4H/fcc and monoclinic structures (i.e., the acanthite α-Ag_2S), respectively (Figure 1c). To further investigate the structure of as-prepared Au@Ag_2S NRBs, high-resolution TEM (HRTEM) characterization was carried out (Figure 1d,e), confirming the coating of the Ag_2S shell on the Au core (Figure 1e). The Au core is dominated by the 4H hexagonal structure, along with short-range fcc domains (Figure 1d,e), consistent with the SAED result (Figure 1c). A lattice spacing of 2.4 Å is attributed to the interplane distance of close-packed planes along the $[001]_{4H}/[111]_f$ directions in the Au core (Figure 1d,e). The Ag_2S shell is polycrystalline, identified by the presence of crystal grain boundaries (Figure 1e). The lattice fringes with interplane distances of 2.6 Å can be assigned to the $\{\bar{1}21\}$ planes of monoclinic Ag_2S (Figure 1e). The chemical composition of Au@Ag_2S NRBs is measured by STEM-EDS, showing an average Au/Ag/S atomic ratio of 1.0/1.1/0.7 (Figure S3). The atomic ratio of Ag/S (1.1/0.7) is slightly deviated from 2.0/1.0, suggesting the presence of excess S adsorbed on the surface of Au@Ag_2S NRBs, which has been observed in the synthesized Ag_2S nanoparticles and films.[10] A typical high-angle annular dark-field-STEM (HAADF-STEM) image and the corresponding STEM-EDS elemental mappings indicate the homogeneous distribution of Au, Ag, and S (Figure 1f−i), which is further verified by the STEM-EDS line scanning profile (Figure S4).

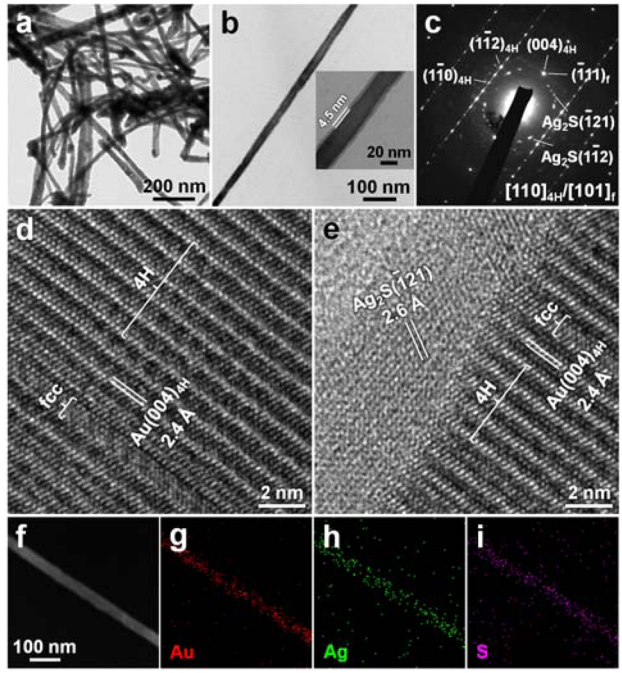

Figure 1. (a) Bright-field TEM image of 4H/fcc-Au@Ag_2S NRBs. (b) TEM image of a typical 4H/fcc-Au@Ag_2S NRB. Inset: Magnified TEM image of the 4H/fcc-Au@Ag_2S NRB. (c) The corresponding SAED pattern of a 4H/fcc-Au@Ag_2S NRB taken along the $[110]_{4H}/[101]_f$ zone axes of Au core. The other randomly distributed diffraction spots arise from the polycrystalline Ag_2S shell. (d,e) HRTEM images of a 4H/fcc-Au@Ag_2S NRB taken in its center (d) and at its edge (e). (f) A typical HAADF-STEM image and (g−i) the corresponding STEM-EDS elemental mappings of a 4H/fcc-Au@Ag_2S NRB.

Importantly, as shown in Scheme 1, the obtained 4H/fcc-Au@Ag_2S NRBs could be used to synthesize a series of 4H/fcc-Au@MS (M = Cd, Pb, or Zn) NRB heterostructures through the cation exchange in the presence of tributylphosphine (TBP). Note that TBP is a soft base, which binds much more tightly to the monovalent ions (such as Ag^+) compared to the divalent metal ions (such as Cd^{2+}, Pb^{2+}, or Zn^{2+}). Therefore, the addition of small amount of TBP can promote the cation exchange of Ag^+ ions with Cd^{2+}, Pb^{2+}, or Zn^{2+} in 4H/fcc-Au@Ag_2S NRBs.[4c,e] As a typical example, the 4H/fcc-Au@CdS NRB heterostructure was synthesized from the 4H/fcc-Au@Ag_2S NRB via the cation exchange of Ag^+ ions with excess Cd^{2+} in the presence of TBP at 55 °C (see the Experimental Section in Supporting Information for details). The core−shell architecture is preserved after the cation exchange of Ag^+ with Cd^{2+} ions in the Au@Ag_2S NRBs (Figure 2a−c). The average thickness of resulting CdS shell is about 3.8 nm (Figure 2c). The chemical composition of Au@CdS NRBs is measured by STEM-EDS, showing average Au/Cd/S atomic ratio of 1.0/0.5/0.4 (Figure S5), which reveals that the surface of CdS shell is Cd-rich.[11] HAADF-STEM image of an Au@CdS NRB and the corresponding STEM-EDS elemental mappings indicate the uniform distribution of Au, Cd, and S (Figure 2f−i), which is further confirmed by the STEM-EDS line scanning analysis (Figure S6). Importantly, SAED pattern shows that the

DOI: 10.1021/jacs.5b06405
J. Am. Chem. Soc. 2015, 137, 10910−10913

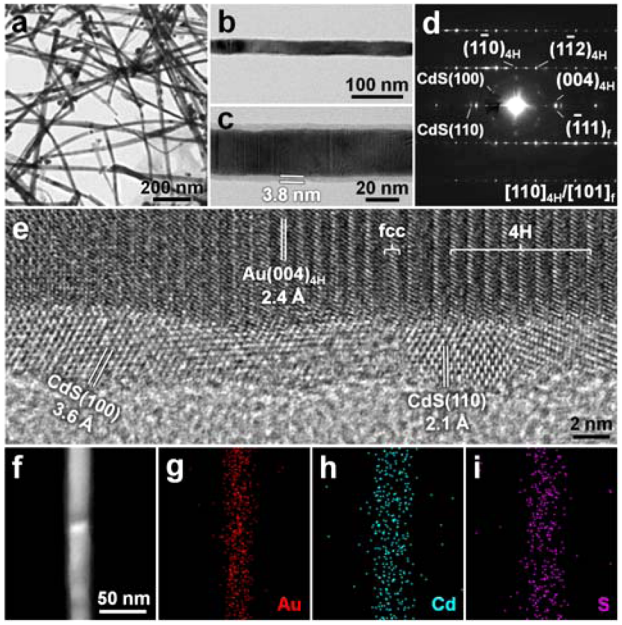

Figure 2. (a) Bright-field TEM image of 4H/fcc-Au@CdS NRBs. (b,c) Magnified TEM images of a typical 4H/fcc-Au@CdS NRB. (d) The corresponding SAED pattern of a 4H/fcc-Au@CdS NRB taken along the $[110]_{4H}/[101]_f$ zone axes of Au core. The other randomly distributed diffraction spots arise from the polycrystalline CdS shell. (e) A typical HRTEM image of the 4H/fcc-Au@CdS NRB. (f) HAADF-STEM image and (g–i) the corresponding STEM-EDS elemental mappings of a typical 4H/fcc-Au@CdS NRB.

alternating 4H/fcc structure of the Au core is well-maintained and the CdS shell crystallizes in the wurtzite hexagonal structure (Figure 2d). No diffraction spots belonging to the α-Ag_2S can be observed in the SAED pattern of an Au@CdS NRB derived from the Au@Ag_2S NRB, suggesting the successful transformation of α-Ag_2S to wurtzite CdS after the cation exchange of Ag^+ with Cd^{2+} ions. HRTEM image further confirms the coexistence of alternating 4H and fcc structures in the Au core, and the formation of a polycrystalline wurtzite CdS shell which is evidenced by the presence of crystal grain boundaries (Figure 2e). The lattice spacings of 3.6 and 2.1 Å can be assigned to the {100} and {110} planes of hexagonal CdS, respectively. Interestingly, TEM image of Au@CdS NRB also shows the Moiré patterns, which are caused by the interference of the two mismatched crystal lattices of the Au core and CdS shell (Figure S7).

Furthermore, through the cation exchange of Ag^+ with excess Pb^{2+} or Zn^{2+} ions in the presence of TBP, the 4H/fcc-Au@PbS or 4H/fcc-Au@ZnS NRB heterostructures can be prepared from the obtained 4H/fcc-Au@Ag_2S NRBs, respectively (Figure 3 and Figures S8–S15). Figure 3a,b shows the typical TEM images of the as-prepared Au@PbS NRBs. The PbS shell, with average thickness of about 6.0 nm, is coated on the Au core (Figure 3b). The Au core in Au@PbS NRBs shows the alternating 4H/fcc structure (Figure 3c,d). The PbS shell crystallizes in the rock-salt cubic structure, which shows a polycrystalline feature (Figure 3c,d). The lattice spacings of 3.5 and 3.0 Å can be attributed to the interplane distances of {111} and {200} planes of cubic PbS, respectively (Figure 3d). Figure 3e,f shows the TEM images of the obtained Au@ZnS NRBs. The ZnS shell has average thickness of about 4.2 nm (Figure 3f). Similar to the aforementioned Au@CdS NRB (Figure 2d,e), the Au core and ZnS shell in the obtained Au@ZnS NRB also show the alternating 4H/fcc and wurtzite hexagonal structures, respectively (Figure 3g,h). HRTEM image confirms the presence of crystal grain boundaries, suggesting the polycrystalline feature of the ZnS shell (Figure 3h). The lattice fringes with interplane spacings of 3.3 and 2.0 Å can be assigned to the {100} and {110} planes of hexagonal ZnS, respectively (Figure 3h). All the aforementioned results demonstrated that a series of 4H/fcc-Au@MS (M = Cd, Pb, or Zn) NRBs have been successfully prepared from the 4H/fcc-Au@Ag_2S NRBs through the cation exchange reaction.

In summary, for the first time, a novel class of 4H/fcc-Au@metal sulfide core–shell NRB heterostructures has been successfully synthesized from the 4H/fcc Au@Ag NRBs. The

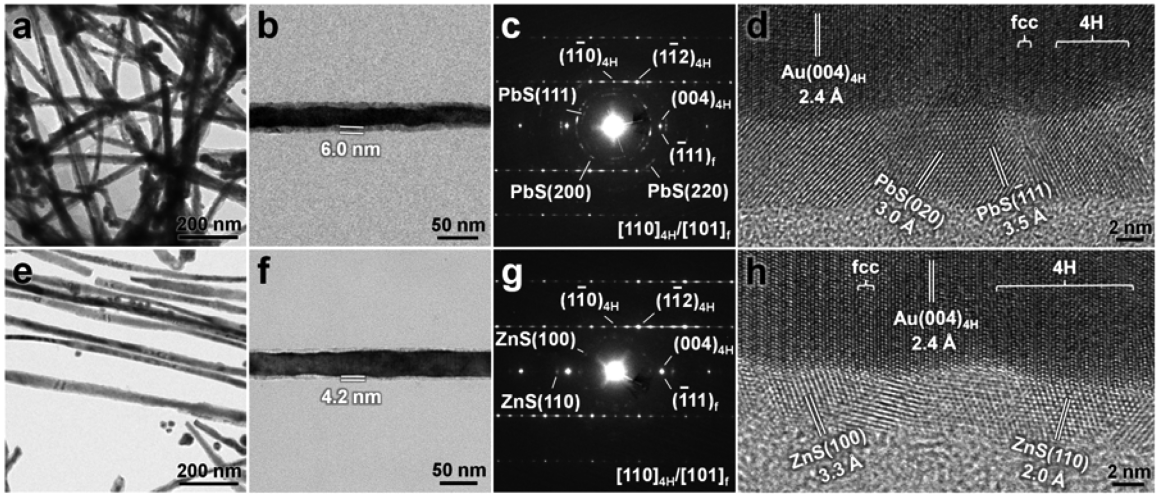

Figure 3. (a) Bright-field TEM image of 4H/fcc-Au@PbS NRBs. (b) Magnified TEM image of a typical 4H/fcc-Au@PbS NRB. (c) The corresponding SAED pattern of a 4H/fcc-Au@PbS NRB acquired along the $[110]_{4H}/[101]_f$ zone axes of Au core. The other randomly distributed diffraction spots are attributed to the polycrystalline PbS shell. (d) A typical HRTEM image of a 4H/fcc-Au@PbS NRB. (e) Bright-field TEM image of 4H/fcc-Au@ZnS NRBs. (f) Magnified TEM image of a typical 4H/fcc-Au@ZnS NRB. (g) The corresponding SAED pattern of a 4H/fcc-Au@ZnS NRB acquired along the $[110]_{4H}/[101]_f$ zone axes of Au core. The other randomly distributed diffraction spots are attributed to the polycrystalline ZnS shell. (h) A typical HRTEM image of a 4H/fcc-Au@ZnS NRB.

DOI: 10.1021/jacs.5b06405
J. Am. Chem. Soc. 2015, 137, 10910–10913

metal sulfide shells are polycrystalline nanostructures. These novel 4H/fcc-Au@metal sulfide heteronanostructures may open up new opportunities for various applications in catalysis, SERS, solar cells, photothermal therapy, etc.

■ ASSOCIATED CONTENT

Supporting Information

The Supporting Information is available free of charge on the ACS Publications website at DOI: 10.1021/jacs.5b06405.

Materials, detailed experimental methods, TEM images, and EDS analyses (PDF)

■ AUTHOR INFORMATION

Corresponding Author

*hzhang@ntu.edu.sg

Notes

The authors declare no competing financial interest.

■ ACKNOWLEDGMENTS

This work was supported by MOE under AcRF Tier 2 (ARC 26/13, No. MOE2013-T2-1-034; ARC 19/15, No. MOE2014-T2-2-093) and AcRF Tier 1 (RGT18/13, RG5/13), and NTU under Start-Up Grant (M4081296.070.500000) in Singapore. This Research is also conducted by NTU-HUJ-BGU Nanomaterials for Energy and Water Management Programme under the Campus for Research Excellence and Technological Enterprise (CREATE), that is supported by the National Research Foundation, Prime Minister's Office, Singapore.

■ REFERENCES

(1) (a) Linic, S.; Christopher, P.; Ingram, D. B. *Nat. Mater.* **2011**, *10*, 911. (b) Jiang, R.; Li, B.; Fang, C.; Wang, J. *Adv. Mater.* **2014**, *26*, 5274. (c) Banin, U.; Ben-Shahar, Y.; Vinokurov, K. *Chem. Mater.* **2014**, *26*, 97. (d) Lin, C. W.; Pan, T. S.; Chen, M. C.; Yang, Y. J.; Tai, Y.; Chen, Y. F. *Appl. Phys. Lett.* **2011**, *99*, 023303. (e) Huang, X.; Zeng, Z.; Bao, S.; Wang, M.; Qi, X.; Fan, Z.; Zhang, H. *Nat. Commun.* **2013**, *4*, 1444.

(2) (a) Tada, H.; Mitsui, T.; Kiyonaga, T.; Akita, T.; Tanaka, K. *Nat. Mater.* **2006**, *5*, 782. (b) Li, P.; Wei, Z.; Wu, T.; Peng, Q.; Li, Y. *J. Am. Chem. Soc.* **2011**, *133*, 5660. (c) Mubeen, S.; Lee, J.; Singh, N.; Kramer, S.; Stucky, G. D.; Moskovits, M. *Nat. Nanotechnol.* **2013**, *8*, 247. (d) Fan, Z.; Huang, X.; Han, Y.; Bosman, M.; Wang, Q.; Zhu, Y.; Liu, Q.; Li, B.; Zeng, Z.; Wu, J.; Shi, W.; Li, S.; Gan, C. L.; Zhang, H. *Nat. Commun.* **2015**, *6*, 6571. (e) Fan, Z.; Huang, X.; Tan, C.; Zhang, H. *Chem. Sci.* **2015**, *6*, 95.

(3) (a) Seh, Z. W.; Liu, S.; Zhang, S.-Y.; Bharathi, M. S.; Ramanarayan, H.; Low, M.; Shah, K. W.; Zhang, Y.-W.; Han, M.-Y. *Angew. Chem.* **2011**, *123*, 10322. (b) Kuo, C.-H.; Hua, T.-E.; Huang, M. H. *J. Am. Chem. Soc.* **2009**, *131*, 17871. (c) Lee, J.-S.; Shevchenko, E. V.; Talapin, D. V. *J. Am. Chem. Soc.* **2008**, *130*, 9673. (d) Ye, X.; Reifsnyder Hickey, D.; Fei, J.; Diroll, B. T.; Paik, T.; Chen, J.; Murray, C. B. *J. Am. Chem. Soc.* **2014**, *136*, 5106. (e) Wang, H.; Sun, Z.; Lu, Q.; Zeng, F.; Su, D. *Small* **2012**, *8*, 1167.

(4) (a) Gupta, S.; Kershaw, S. V.; Rogach, A. L. *Adv. Mater.* **2013**, *25*, 6923. (b) Rivest, J. B.; Jain, P. K. *Chem. Soc. Rev.* **2013**, *42*, 89. (c) Son, D. H.; Hughes, S. M.; Yin, Y.; Paul Alivisatos, A. *Science* **2004**, *306*, 1009. (d) Camargo, P. H. C.; Lee, Y. H.; Jeong, U.; Zou, Z.; Xia, Y. *Langmuir* **2007**, *23*, 2985. (e) Zhang, J.; Tang, Y.; Lee, K.; Ouyang, M. *Science* **2010**, *327*, 1634. (f) Zhang, B.; Jung, Y.; Chung, H.-S.; Vugt, L. V.; Agarwal, R. *Nano Lett.* **2010**, *10*, 149.

(5) (a) Jain, P. K.; Amirav, L.; Aloni, S.; Alivisatos, A. P. *J. Am. Chem. Soc.* **2010**, *132*, 9997. (b) Li, H.; Zanella, M.; Genovese, A.; Povia, M.; Falqui, A.; Giannini, C.; Manna, L. *Nano Lett.* **2011**, *11*, 4964.

(6) Robinson, R. D.; Sadtler, B.; Demchenko, D. O.; Erdonmez, C. K.; Wang, L.-W.; Alivisatos, A. P. *Science* **2007**, *317*, 355.

(7) Huang, X.; Li, S.; Huang, Y.; Wu, S.; Zhou, X.; Gan, C. L.; Boey, F.; Mirkin, C. A.; Zhang, H. *Nat. Commun.* **2011**, *2*, 292.

(8) Fan, Z.; Bosman, M.; Huang, X.; Huang, D.; Yu, Y.; Ong, K. P.; Akimov, Y. A.; Wu, L.; Li, B.; Wu, J.; Huang, Y.; Liu, Q.; Png, C. E.; Gan, C. L.; Yang, P.; Zhang, H. *Nat. Commun.* **2015**, *6*, 7684.

(9) Fan, Z.; Zhu, Y.; Huang, X.; Han, Y.; Wang, Q.; Liu, Q.; Huang, Y.; Gan, C. L.; Zhang, H. *Angew. Chem., Int. Ed.* **2015**, *54*, 5672.

(10) (a) Kim, B.; Park, C.-S.; Murayama, M.; Hochella, M. F. *Environ. Sci. Technol.* **2010**, *44*, 7509. (b) Kundu, M.; Terabe, K.; Hasegawa, T.; Aono, M. *J. Appl. Phys.* **2006**, *99*, 103501. (c) Chen, R.; Noel, T. N.; Laura, M.; Hannah, R. M.; Paul, M. W. *Nanotechnology* **2008**, *19*, 455604.

(11) Li, Z.; Ji, Y.; Xie, R.; Grisham, S. Y.; Peng, X. *J. Am. Chem. Soc.* **2011**, *133*, 17248.

DOI: 10.1021/jacs.5b06405
J. Am. Chem. Soc. 2015, 137, 10910−10913